MAGNETOHYDRODYNAMICS Vol. 59 (2023), No. 3-4, pp. 379–389
DOI: 10.22364/mhd.59.3-4.10

SURFACE DEFORMATIONS OF LIQUID METAL FLOW IN POROUS MEDIA IN EXTERNAL UNIFORM MAGNETIC FIELD

D. Berenis, I. Grants, L. Buligins*

Institute of Physics, University of Latvia, 32 Miera str., LV-2169, Salaspils, Latvia
** e-Mail: didzis.berenis@lu.lv*

A direct numerical simulation of liquid metal flow in an external uniform magnetic field was performed for the cases of three and six cells, which are assumed to be part of a porous material. Free-surface deformations were studied in terms of the external magnetic field direction and strength and in terms of the pressure drop which was applied perpendicular to the direction of gravitation. Numerical results showed that the magnetic field in the direction of the pressure drop is most effective to decrease the height difference between the inlet and the outlet. In contrast, the magnetic field directed perpendicular to the pressure drop and gravitation produced the largest height difference.
Keywords: liquid metals, free-surface, MHD, plasma facing components, fusion reactors.

Introduction. Due to the very harsh conditions which the plasma facing components (PFCs) must withstand in magnetic fusion reactors, a proposition has been made to introduce a liquid metal (LM) free-surface layer [1]. The LM layer could potentially be introduced and supported by utilizing porous materials [2]. Additionally, magnetic fields via the Lorentz force could stabilize and shape the LM surface [3]. An important part of using LMs for the PFCs is to maintain the LM layer which would mitigate the damage to the solid components of the walls [1]. On the other hand, high LM velocities should be maintained to decrease the LM exposure time and, thus, limit the plasma contamination [1]. At the same time, surface instabilities should be minimized to avoid LM droplets splashing in the plasma [4]. Numerical studies of LM PFCs often use porous media modelling techniques to study the global characteristics of PFCs [2, 4]. Instead, in this study, we have performed a direct numerical simulation to investigate the LM free-surface flow around individual cells in an external magnetic field. On the scale of porous cells, the current study advances the general knowledge of the system and could be beneficial for determining which direction of the magnetic field relative to the LM velocity and gravitation direction is preferable to maintain the desirable LM free-surface conditions.

1. Formulation and methods.

CFD calculations were performed with the OpenFOAM software (https://openfoam.org/). A structured mesh, where each cell consisted of 40 000 volume elements, was used (Fig. 1*a*). A pressure difference between the inlet and outlet (Fig. 1*b*) boundaries was applied. The top, bottom, and side boundaries were set to slip, and the pore walls to no-slip boundary conditions (BCs). In two-phase calculations, the top boundary sets the ambient pressure to represent the experimental setup (Fig. 1*c*).

The ElmerFEM software (http://www.elmerfem.org/) along with the EOF-Library [5], which works as a communication between OpenFOAM and ElmerFEM, were applied. Simulations were made similarly as in [6], where the numerical model is described in more detail. In the current study, a two-phase simulation was performed, and only laminar flow was considered. Since ElmerFEM considers the conductivity distribution calculated

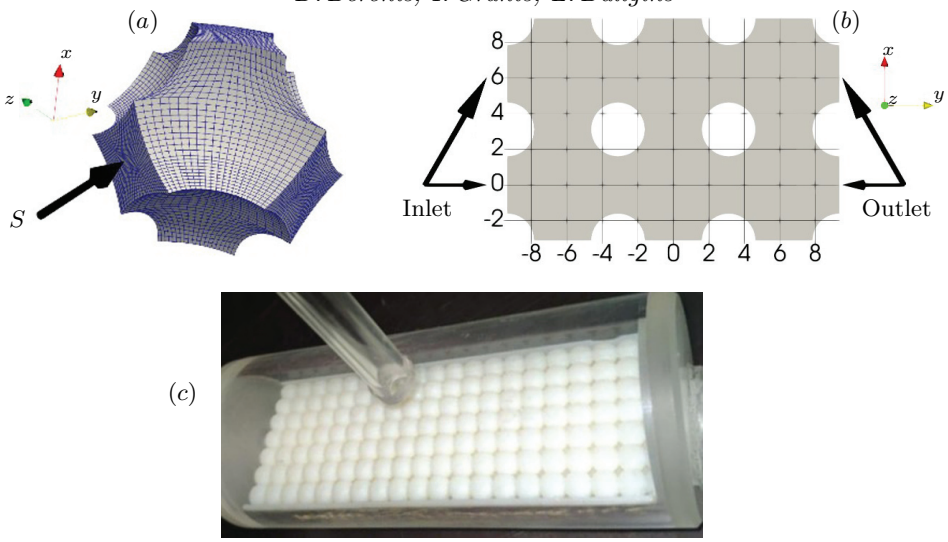

Fig. 1. The porous domain: (*a*) OpenFOAM calculation mesh (shown for one cell); (*b*) inlet and outlet positions in a 6-cell numerical model; (*c*) analogous experimental setup.

by OpenFOAM, the typically used EOF-Library setting for updating electromagnetics (whenever the maximum relative velocity change in a volume element exceeds 50%) was not appropriate because the velocity variation was much slower than the surface deformations, which leads to non-physical results. Thus, the parameter was decreased to 5%. Surface tension was set to zero to decrease the computational difficulty of the study. Physically, it represents the Weber number $\gg 1$, and this requirement was sufficiently fulfilled in the model setup. Additionally, it represents the situation in fusion reactor PFCs, when due to the large heat flow the LM surface reaches the boiling point.

The characteristic length is defined as $L = 0.5\sqrt{S}$, where S is the surface area of the cell boundary (Fig. 1*a*). For result presentation, the length, time, pressure, and the flow rate were scaled according to L, L^2/η_{liqm}, $\rho_{\text{liqm}}\eta_{\text{liqm}}^2/L^2$, and $L\eta_{\text{liqm}}$, respectively. Then, the dimensionless velocity $\mathbf{v}$ is obtained by scaling the velocity with η_{liqm}/L. The Reynolds number (Re) is defined as the maximum $\mathbf{v}$ in the liquid phase. A set of uniform external magnetic field values $B = [0, 1, 2, 3, 4]$ T was used in the parametric calculation which correspond to Hartmann numbers $Ha = BL\sqrt{\sigma/\eta_{\text{liqm}}\rho_{\text{liqm}}} = [0, 3.38, 6.76, 10.15, 13.53]$, respectively. The dimensionless pressure P, ranging $P = [13 : 535]$, was set at the inlet.

Table 1. Geometrical and material parameters.

Parameter	Symbol	Value
Liquid phase viscosity	η_{liqm}	3.35×10^{-7} m^2/s
Liquid phase density	ρ_{liqm}	6400 kg/m^3
Gaseous phase viscosity	η_{air}	1.51×10^{-5} m^2/s
Gaseous phase density	ρ_{air}	1.420 kg/m^3
Surface tension	γ	0 N/m
Electrical conductivity of liquid	σ	3.27×10^{6} S/m
Free fall acceleration	$\mathbf{g}$	(–9.81, 0, 0) m/s^2
Characteristic length	L	8.66×10^{-5} m
Cell side length	–	5.4×10^{-4} m

2. Results.

Initially, a steady-state calculation was performed for a single-phase setup without the external magnetic field (Fig. 2*a*, Fig. 3*a*). Next, a steady-state single-phase calcula-

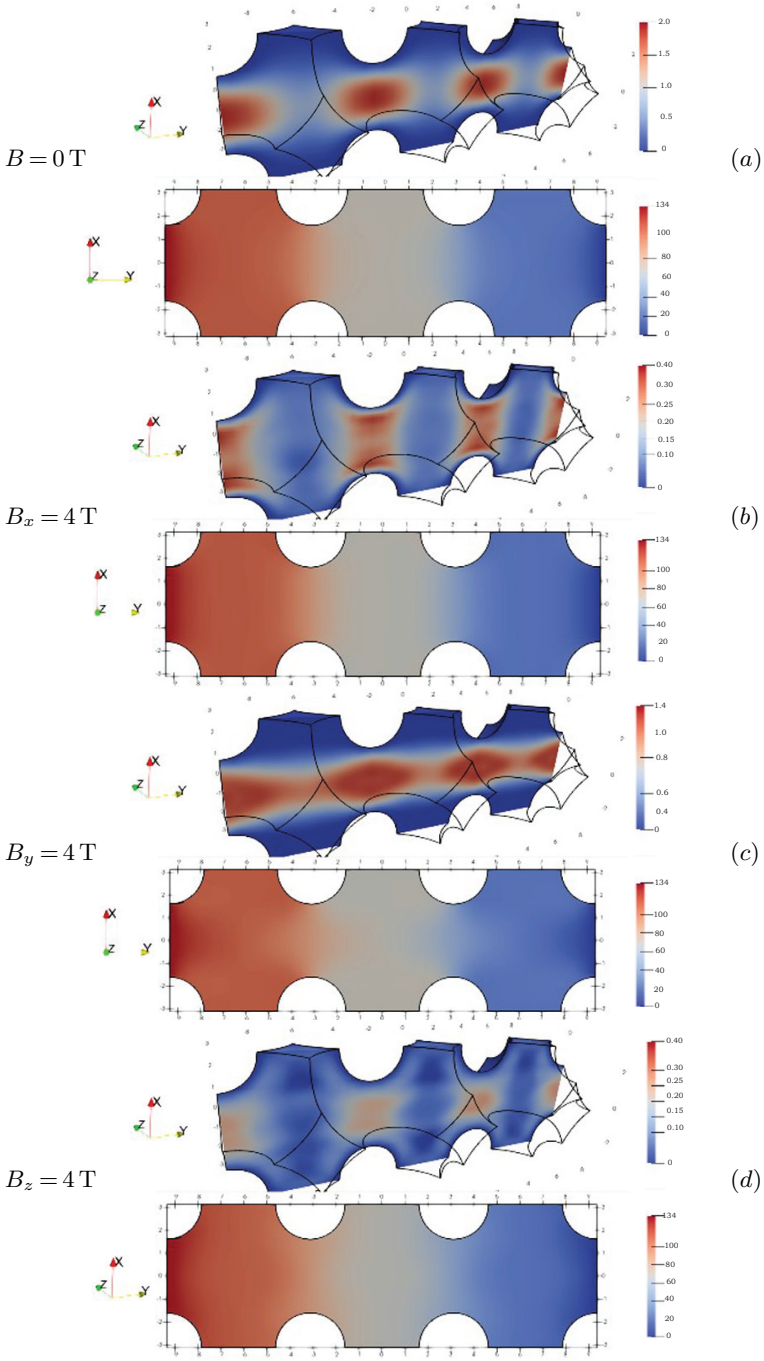

Fig. 2. Dimensionless velocity and pressure distribution for one-phase steady-state simulation with the inlet-to-outlet pressure drop $P = 134$.

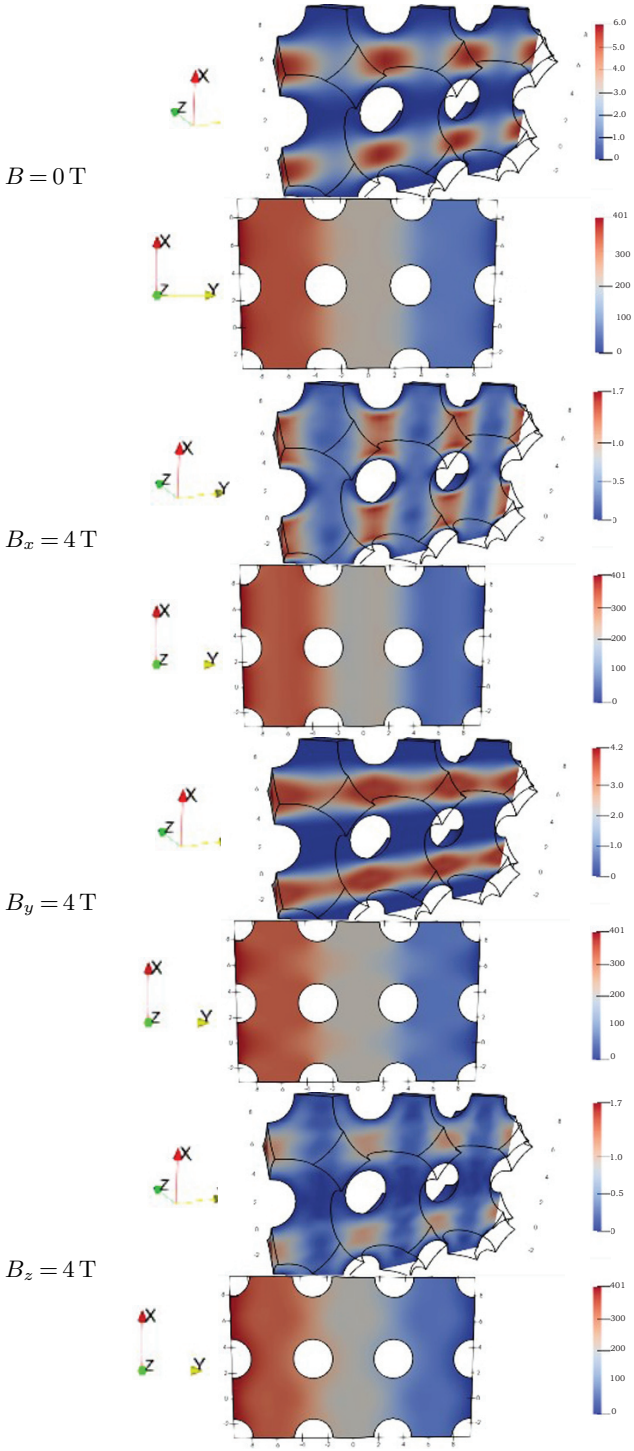

Fig. 3. Dimensionless velocity and pressure distribution for one-phase steady-state simulation with the inlet-to-outlet pressure drop $P = 401$

tion was performed with the external magnetic field in the x-,y-,z-directions (Fig. 2*b–d*, Fig. 3*b–d*). In the two-phase transient simulation with the one row (three cell) geometry (Fig. 4) a set of pressures $P = [13,\ 67,\ 134]$ was used for parametric calculation. For

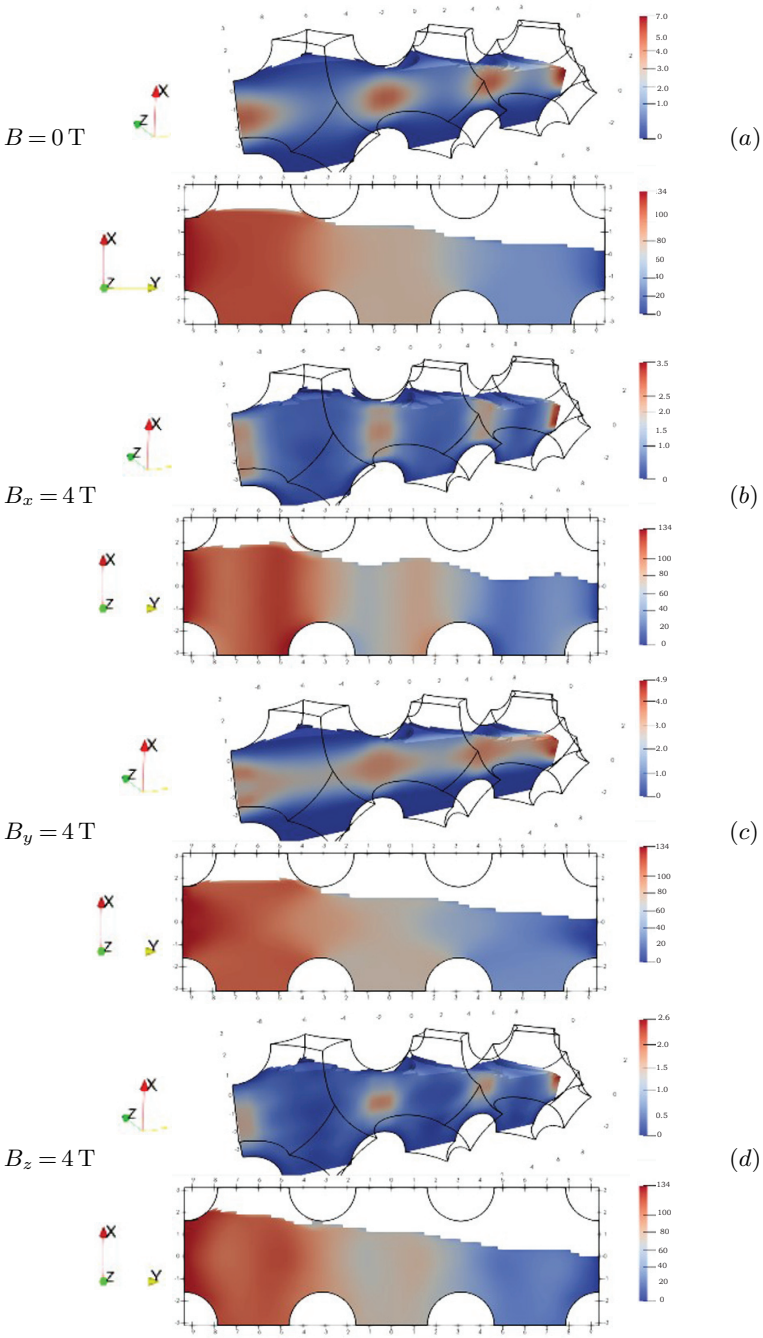

Fig. 4. Dimensionless velocity and pressure distribution for two-phase transient simulation with the inlet-to-outlet pressure drop $P = 134$.

the two row (six cell) geometry (Figs. 5–7), a set of dimensionless pressures $P = [200, 267, 334, 401, 468, 535]$ was used. In hindsight, covering the whole pressure range with the two-row geometry would have facilitated the result interpretation, but due to time

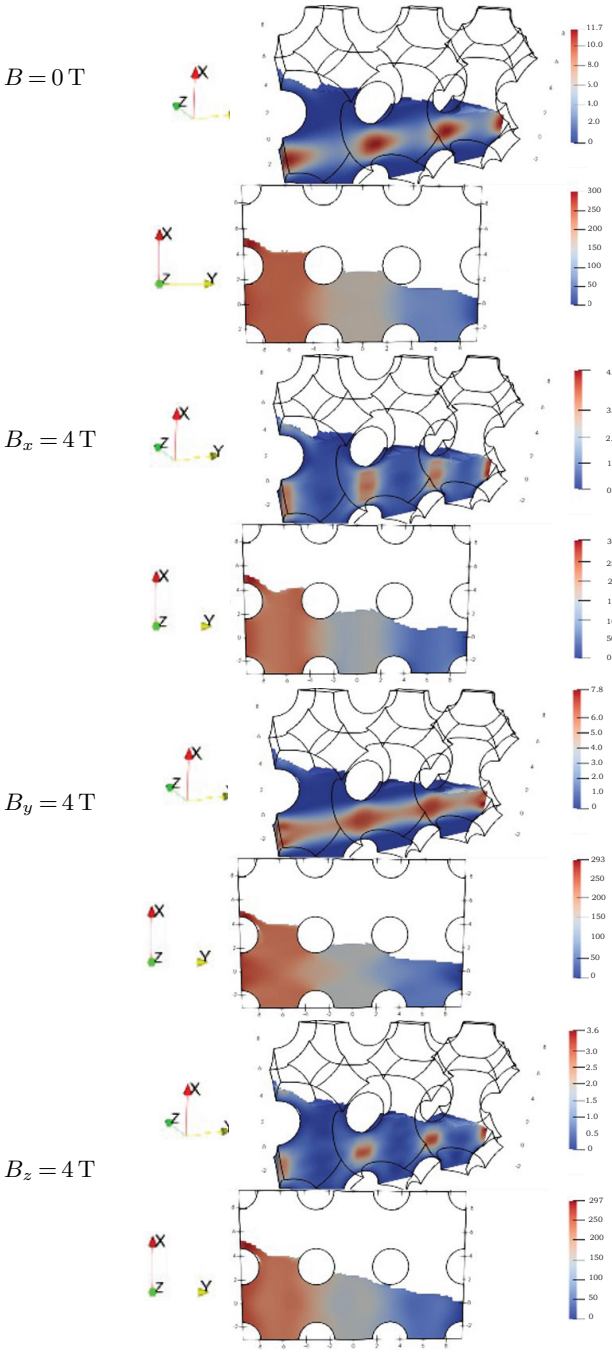

Fig. 5. Dimensionless velocity and pressure distribution for two-phase transient simulation with the inlet-to-outlet pressure drop $P = 267$.

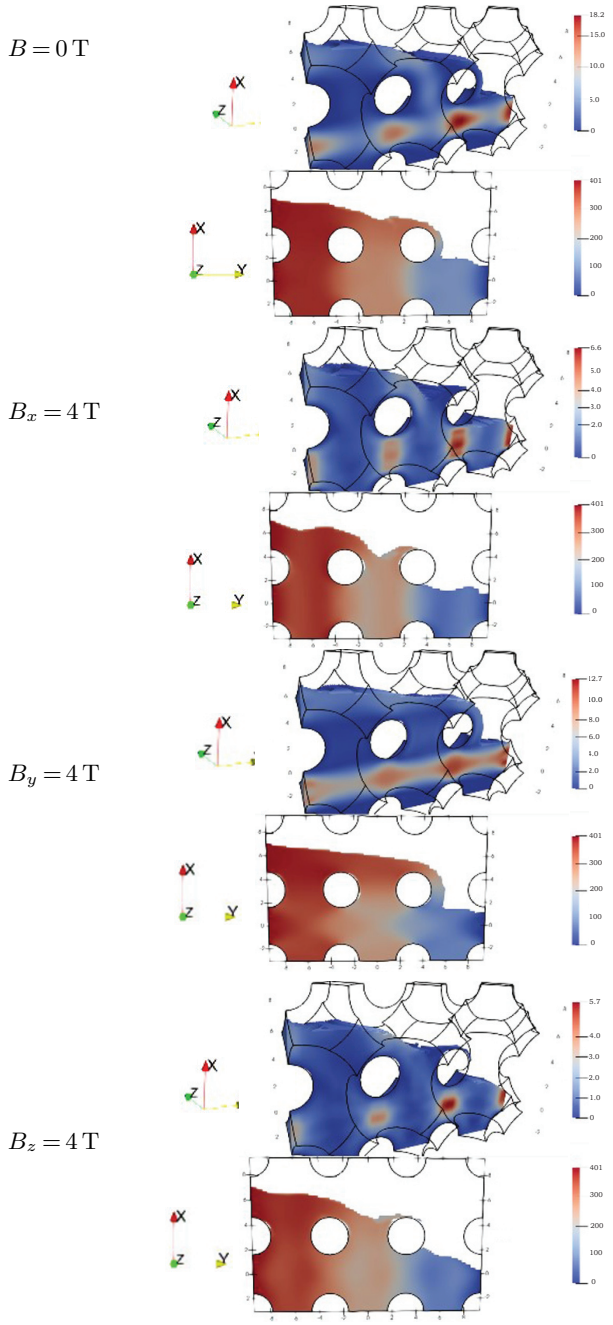

Fig. 6. Dimensionless velocity and pressure distribution for two-phase transient simulation with the inlet-to-outlet pressure drop $P = 401$.

limitations, the one-row pressure range calculations were not repeated with the two-row geometry. Comparing two-phase and one-phase simulation results, the effect of introducing a magnetic field is similar in terms of the velocity distribution in the liquid phase. However, in the two-phase simulation, the maximum velocity increases due to the height

difference between the inlet and the outlet. Applying a magnetic field in the direction of the main flow (Fig. 4*c*, Fig. 5*c*, Fig. 6*c*, Fig. 7*c*) results in a surface profile which is like in the case without the external magnetic field (Fig. 4*a*, Fig. 5*a*, Fig. 6*a*, Fig. 7*a*). On the other hand, applying a magnetic field perpendicular to the main flow direction

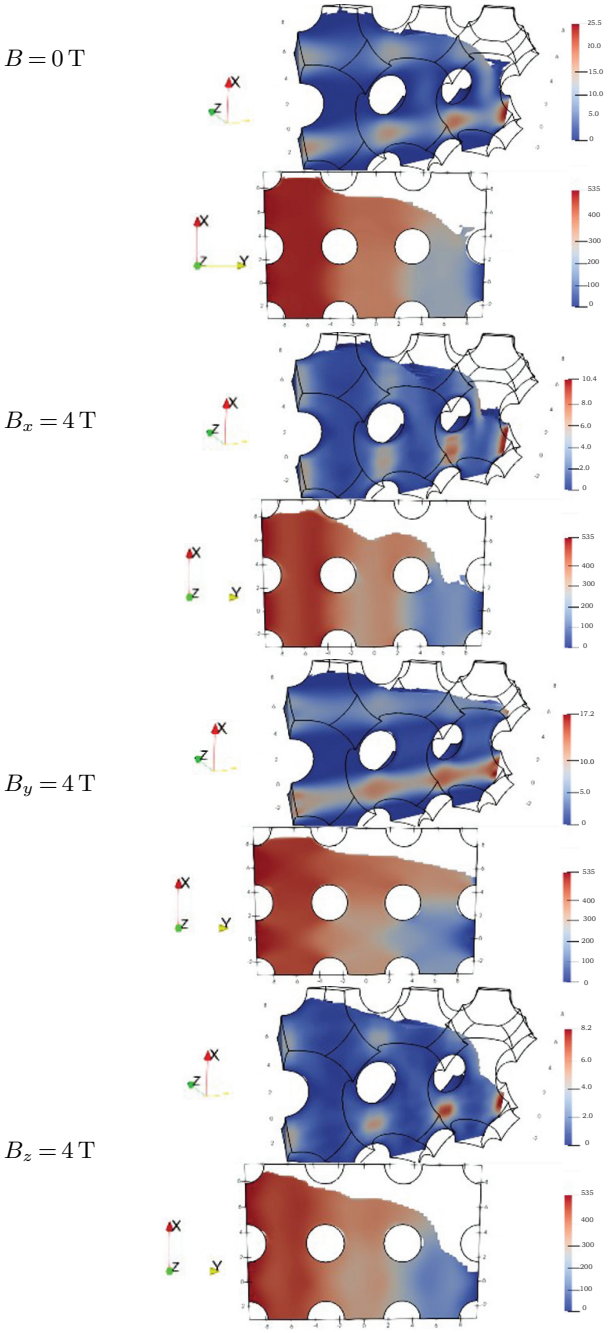

Fig. 7. Dimensionless velocity and pressure distribution for two-phase transient simulation with the inlet-to-outlet pressure drop $P = 535$.

(Fig. 4*b*,*d*, Fig. 5*b*,*d*, Fig. 6*b*,*d*, Fig. 7*b*,*d*) results in a different surface deformation when more of the solid walls' surfaces are uncovered.

In Fig. 8 we have compared the flowrate and pressure drop curves for the one-phase steady-state simulations (Fig. 8*a*) and for the two-phase transient simulations (Fig. 8*b*). Here, the flowrate was calculated to the equivalent for the two-row geometry. In steady-

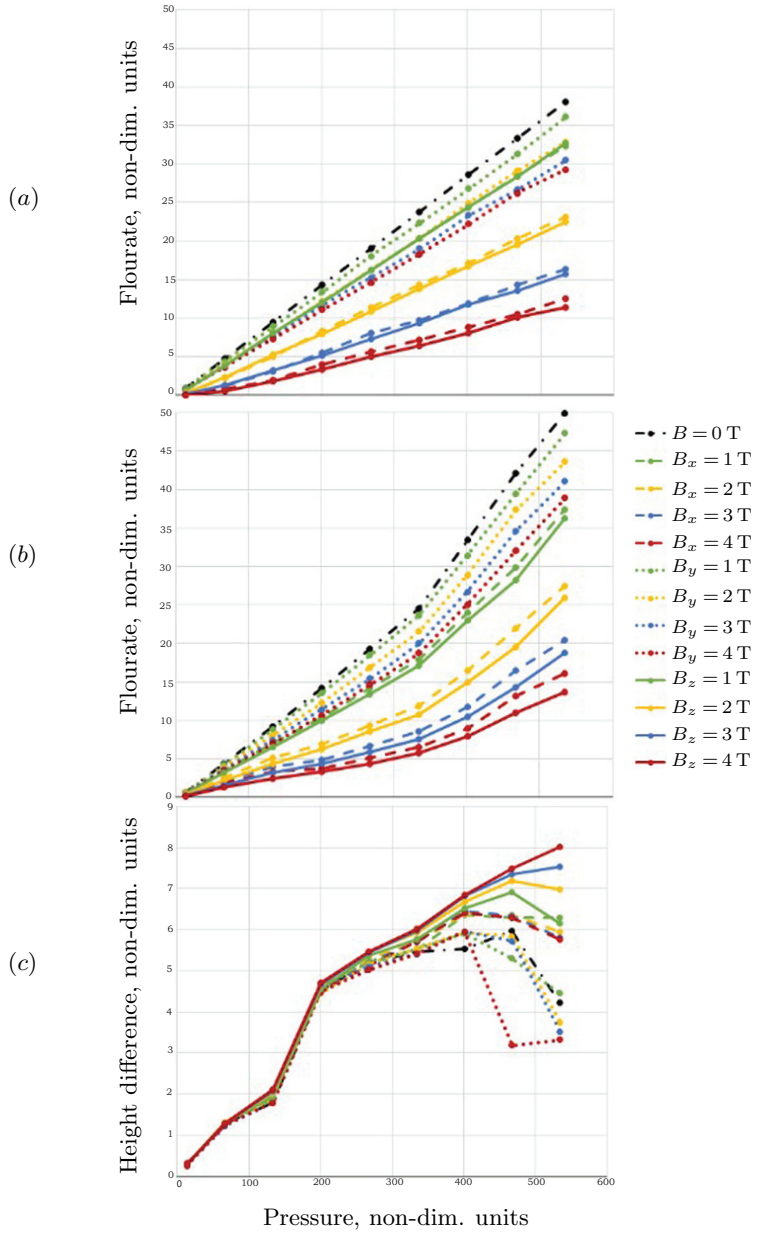

Fig. 8. (*a*) Flowrate dependence on the inlet pressure in one-phase steady-state simulations, and (*b*) two-phase transient simulations. (*c*) Height difference dependence on the inlet pressure in two-phase transient simulations.

state simulations, the magnetic field in the flow direction (y-direction) affects the flowrate the least. External magnetic fields in the direction perpendicular to the flow (x- and z-direction) affect the flow in the same way.

Gravity in this setup is in the negative x-direction, so the magnetic field perpendicular to the gravitation (in the z-direction) produces a stronger braking effect on the flow than the magnetic field in the direction of gravitation (x-direction).

Additionally, the height difference between the inlet and the outlet was calculated (Fig. 8*c*). Due to the discontinuous inlet and outlet, in practice, the inlet height was calculated as the maximum liquid metal height in the domain, but the outlet height was the liquid metal height at the outlet. In the case when the surface level near the outlet was between the first and the second row, the height was calculated at the closest cell connection between the rows, which is 1.51 dimensionless units from the outlet.

In the two-phase transient simulations (Fig. 8*b*), the flowrate seems to have a different tendency for the smallest pressures. Moreover, there seems to be a jump in the inlet-to-outlet height difference between $P = 134$ and $P = 200$ (Fig. 8*c*). This could be because of the influence of using two different geometries (one-row geometry with three cells for smaller pressures and a two-row one with six cells for larger pressures). However, the sudden changes were most likely due to the liquid reaching the second row.

It is difficult to see a clear dependence on the external magnetic field. The differences at larger pressures could be simply due to the difficulty of precisely calculating the height at the outlet because of some air pockets which might disappear if the simulation was continued for a longer time. Additionally, the inlet height calculation may have been affected by the number of rows in the model, especially when the liquid is near the top boundary (compare, e.g., Fig. 5*a* and Fig. 7*a*). Nonetheless, there are few general tendencies for the choice of the direction of the external magnetic field. The magnetic field in the z-direction results in the largest height difference. In contrast, the inlet-to-outlet height difference stays the same or even slightly decreases when the magnetic field is applied in the y-direction.

In the setup of this study, the pressure drop was applied only perpendicular to the gravitation direction. An additional study would be necessary to investigate surface deformations in the external magnetic field for other relevant angles between gravitation and the applied pressure drop.

3. Conclusions.

It is possible to perform a two-phase direct numerical simulation of liquid flow in a few cells of a porous medium exposed to a uniform external magnetic field.

Qualitatively, the direction and the strength of the magnetic field affect the liquid flow similarly as in a single-phase simulation.

In the two-phase simulation, the magnetic field directed perpendicular to the applied pressure drop and gravitation direction has the strongest braking effect on the flow. Consequently, a larger surface of the solid wall is uncovered compared to the case without the magnetic field. In contrast, the magnetic field parallel to the applied pressure drop has the least braking effect.

The obtained numerical results show that the magnetic field parallel to the applied pressure appears to slightly decrease the height difference between inlet and outlet, whereas the magnetic field directed perpendicularly increases the height difference. However, a clear relationship between the applied pressure difference and the inlet-to-outlet height difference was not observed. Instead, there was a sudden dispersion of the height

differences at higher pressures. Thus, before making more general conclusions, these results should be reexamined, preferably with a larger cell matrix.

4. Acknowledgements.

This study was carried out in the framework of the EUROfusion Consortium funded by the European Union via the Euratom Research and Training Programme (Grant Agreement No. 101052200 EUROfusion). Views and opinions expressed are, however, those of the author(s) only and do not necessarily reflect those of the European Union or the European Commission. Neither the European Union nor the European Commission can be held responsible for them.

References

[1] C.E. Kessel *et al.* Critical exploration of liquid metal plasma-facing components in a fusion nuclear science facility. *Fusion Science and Technology*, vol. 75 (2019), no. 8, 886-917; DOI: 10.1080/15361055.2019.1610685.

[2] A. Khodak, R. Maingi. Modeling of liquid lithium flow in porous plasma facing material. *Nuclear Materials and Energy*, vol. 26 (2021), 100935; DOI: 1016/j.nme.2021.100935.

[3] M.G. Hvasta *et al.* Demonstrating electromagnetic control of free-surface, liquid-metal flows relevant to fusion reactors. *Nucl. Fusion*, vol. 58 (2018), 016022; DOI: 10.1088/1741-4326/aa9344.

[4] J. Rudolph, G. Miloshevsky. Analysis and modeling of lithium flows in porous materials. *Plasma Phys. Rep.*, vol. 44 (2018), pp. 685–691; DOI: 10.1134/S1063780X1807005X.

[5] J. Vencels *et al.* EOF-Library: Open-source Elmer FEM and OpenFOAM coupler for electromagnetics and fluid dynamics. *SoftwareX*, vol. 9 (2019), pp. 68–72; DOI: 10.1016/j.softx.2019.01.007.

[6] A. Gaile *et al.* Permanent magnet pump for aluminum transport in a linear channel. *Metals*, vol. 13 (2023), 1160; DOI: 10.3390/met13071160.

Received 24.11.2023